Stat3 is indispensable for damage-induced crypt regeneration but not for Wnt-driven intestinal tumorigenesis.

著者	Oshima Hiroko, Kok Sau-Yee, Nakayama Mizuho, Murakami Kazuhiro, Voon Dominic Chih-Cheng, Kimura Takashi, Oshima Masanobu
著者別表示	大島 浩子, 中山 瑞穂, 村上 和弘, 大島 正伸
journal or publication title	FASEB journal
volume	33
number	2
page range	1873-1886
year	2019-02-01
URL	http://doi.org/10.24517/00053860

doi: 10.1096/fj.201801176R

Stat3 is indispensable for damage-induced crypt regeneration but not for Wnt-driven intestinal tumorigenesis

Hiroko Oshima*,†, Sau-Yee Kok*, Mizuho Nakayama*,†, Kazuhiro Murakami‡, Dominic Chih-Cheng Voon§, Takashi Kimura¶, Masanobu Oshima*,†

*Division of Genetics, Cancer Research Institute, †WPI Nano-Life Science Institute (Nano-LSI), ‡Division of Stem Cell Biology, Cancer Research Institute, Kanazawa University, Kanazawa, Japan, §Cancer Research Core, Institute for Frontier Science Initiative (InFiniti), Kanazawa University, Kanazawa, Japan, ¶Laboratory of Comparative Pathology, Faculty of Veterinary Medicine, Hokkaido University, Sapporo, Japan.

Corresponding: Masanobu Oshima, Division of Genetics, Cancer Research Institute, Kanazawa University, Kanazawa, 920-1192 Japan.

Phone, 81-76-264-6760; Fax: 81-76-234-4519;

E-mail: oshimam@staff.kanazawa-u.ac.jp

Running title: Stat3 in intestinal regeneration and tumorigenesis

Abbreviations

AFM-Wnt3a, afamin-associated Wnt3a; *Apc*, adenomatous polyposis coli; CAC, colitis-associated colon cancer; CRC, colorectal cancer; DSS, dextran sodium sulfate; ECM, extracellular matrix; EDTA, ethylenediaminetetraacetic acid; EdU, 5-ethynyl-2'-deoxyuridine; FAK, focal adhesion kinase; GSK, glycogen synthase kinase; IL, interleukin; ROCK, Rho-associated protein kinase, RT-PCR, reverse transcription polymerase chain reaction; Stat3, signal transducer and activator of transcription 3; TGF-β; transforming growth factor-β

ABSTRACT

Stat3 has been shown to play a role in intestinal regeneration and colitis-associated colon carcinogenesis. However, the role of Stat3 in the Wnt-driven sporadic intestinal tumorigenesis remains poorly understood. We examined the roles of Stat3 in intestinal regeneration and tumorigenesis by organoid culture experiments using *Stat3*$^{\Delta IEC}$ mouse-derived intestinal epithelial cells in which *Stat3* was disrupted. The regeneration of intestinal mucosa and organoid formation were significantly suppressed by *Stat3* disruption, which was compensated by Wnt activation. Furthermore, once organoids were recovered, Stat3 was no longer required for organoid growth. These results indicate that Stat3 and Wnt signaling cooperatively protect epithelial cells at the early phase of intestinal regeneration. In contrast, intestinal tumorigenesis was not suppressed by *Stat3* disruption in *Apc*$^{\Delta 716}$ and *Apc*$^{\Delta 716}$ *Tgfbr2*$^{\Delta IEC}$ mice, thus indicating that Stat3 is not required for Wnt activation-driven intestinal tumorigenesis. Mechanistically, *Itga5* and *Itga6* were downregulated by *Stat3* disruption, and FAK activation was also suppressed. Notably, FAK inhibitor suppressed the organoid formation of wild-type epithelial cells. These results indicate that Stat3 is indispensable for the survival of epithelial cells through the activation of integrin signaling and the downstream FAK pathway; however, it is not required for the Wnt signaling-activated normal or tumor epithelial cells.

KEY WORDS: colon cancer, organoids, anoikis, integrin, FAK,

INTRODUCTION

It has been established that inflammatory responses promote cancer development and malignant progression (1, 2). In the inflammatory tumor microenvironment, macrophages and fibroblasts express cytokines and chemokines, resulting in the activation of transcription factors, such as NF-κB and signal transducer and activator of transcription 3 (Stat3). The aberrant activation of Stat3 was found in >70% of human cancers (3, 4), and Stat3 activation is correlated with the invasiveness, proliferation and stemness of human colon cancer cells (5-7). Furthermore, studies using a colitis-associated colon cancer (CAC) mouse model have shown that the disruption of *Stat3* in epithelial cells significantly suppresses CAC development through the suppression of proliferation and induction of apoptosis (8, 9). It has also been shown that IL-11 is a dominant IL-6 family cytokine in gastrointestinal tumors, and IL-11 receptor signaling promotes tumorigenesis through Stat3 activation (10). Based on these results, the Stat3 pathway is thought to be an important target in the development of anti-cancer drugs for various cancers, including CRC (11).

In contrast to these findings, several studies have demonstrated a tumor suppressor role of Stat3 in intestinal tumorigenesis (12, 13). In those reports, the disruption of *Stat3* in Apc^{Min} mice, a model of familial adenomatous polyposis, did not suppress tumorigenesis; instead, it induced the submucosal invasion of tumor cells, suggesting that Stat3 prevents the malignant progression of intestinal tumors. This discrepancy in the role of Stat3 in intestinal tumorigenesis may be due to the different mechanisms of cancer development in these models (i.e. inflammation and regeneration-associated tumorigenesis in the CAC model and Wnt activation-driven tumorigenesis in Apc^{Min} mice). A comprehensive genome analysis indicated that >90% of human CRCs carry genetic alterations in *APC* or *CTNNB1* resulting in Wnt

signaling activation (14); thus, it is important to investigate the precise role of Stat3 in Wnt activation-driven CRC development.

The Stat3 function has been shown to be absolutely required for the intestinal stem cell survival (15). Consistently, Stat3 plays a role in the regeneration of the damaged intestinal mucosa after irradiation or DSS treatment (16, 17). However, the mechanism through which Stat3 signaling is involved in the stem cell survival and proliferation during regeneration has not been fully elucidated. Wnt/β-catenin signaling is a key driver of the tissue stem cell property, making the Wnt pathway important for both regeneration and cancer development (18, 19). Furthermore, pathways through focal adhesion kinase (FAK) or lysin methyltransferase SETD7 are responsible for both mucosal regeneration and tumorigenesis in the intestine through the activation of Wnt signaling (20, 21). However, the role of Stat3 in intestinal regeneration and tumorigenesis has not been studied in the context of Wnt-driven carcinogenesis.

In the present study, we used genetic mouse models and organoid culture systems to show that Stat3 is required for the survival and proliferation of the residual stem cells in damaged mucosa or isolated crypts, leading to crypt formation in the regenerating mucosa as well as organoid formation in Matrigel. However, Stat3 is not required for crypt development when Wnt signaling is activated by exogenous ligand stimulation or when the *Apc* gene is lost. Consistently, Stat3 is dispensable for Wnt activation-driven tumor development and malignant progression, including submucosal invasion and liver metastasis. These results suggest that the Wnt activation status and regeneration phenotype are important factors to consider with regard to the efficacy of Stat3 inhibitors in the prevention of CRC development.

MATERIALS AND METHODS

Mouse experiments

Apc$^{\Delta 716}$, *Stat3*$^{flox/flox}$ and *villin-CreER* mice were previously described (22-24). *Tgfbr2*$^{flox/flox}$ mice were obtained from the Mouse Repository (NCI-Frederick, Frederick, MD, USA) (25). The genetic background of all strains used in this study is C57BL/6. For organoid culture experiments, *villin-CreER Stat3*$^{flox/flox}$ mice were treated with Tamoxifen (Tam; 4 mg/mouse, intraperitoneal [i.p.]) for 3 continuous days at 4-8 weeks of age, resulting in *Stat3* disruption in the intestinal epithelial cells (hereafter, *Stat3*$^{\Delta IEC}$). X-ray irradiation (9 Gy) was performed to induce intestinal mucosal regeneration (n=9 for wild-type mice, and n=12 for *Stat3*$^{\Delta IEC}$ mice). For the *in vivo* experiments, *Apc*$^{\Delta 716}$ *villin-CreER Stat3* $^{flox/flox}$ mice and *Apc*$^{\Delta 716}$ *villin-CreER Tgfbr2*$^{flox/flox}$ *Stat3* $^{flox/flox}$ mice were generated by crossing and treated with Tam (4 mg/mouse, i.p.) once per week from 6 to 19 weeks of age. The total number of intestinal polyps and the size distribution were scored under a dissection microscope (n=10 for *Apc*$^{\Delta 716}$ mice, n=12 for *Apc*$^{\Delta 716}$ *Stat3*$^{\Delta IEC}$ mice, n=10 for *Apc*$^{\Delta 716}$ *Tgfbr2*$^{\Delta IEC}$ mice, and n=8 for *Apc*$^{\Delta 716}$ *Tgfbr2*$^{\Delta IEC}$ *Stat3*$^{\Delta IEC}$ mice). Invasion frequency was scored using hematoxylin and eosin (H&E) histology sections (n=4 each for *Apc*$^{\Delta 716}$ and *Apc*$^{\Delta 716}$ *Stat3*$^{\Delta IEC}$ mice).

The protocols for the animal experiments were approved by the Committee on Animal Experimentation of Kanazawa University.

Organoid culture experiments

The organoid cultures were prepared from the intestinal mucosa and tumors of the small intestine according to a previously described method (26). In brief, dissected tissues were soaked in 2 mM EDTA for 30 min, and crypts were isolated by shaking. Isolated crypts were

then collected and suspended in Matrigel with Advanced DMEM/F12 medium (Invitrogen, Carlsbad, CA, USA) supplemented with 50 ng/ml EGF (Invitrogen), 100 ng/ml Noggin (Peprotech, Rocky Hill, NJ, USA) and 10% R-Spondin1 conditioned medium prepared from human R-Spondin1-expressing 293T cells (kindly provided by Nick Barker's lab; A-STAR, Singapore). For mechanical passage, 15 organoids (200 μm < ϕ < 400 μm) were collected using Cell Recovery Solution (CORNING, Corning, NY, USA), and crypt structures roughly dissociated into fragments by pipetting were mixed with Matrigel and transferred to 3 wells of a 48-well plate. For enzymatic passage, the collected organoids were dissociated by treatment with 25 mM trypsin for 5 min, suspended in Matrigel, and seeded at 10^5 cells/well (for wild-type and *Stat3*$^{\Delta IEC}$ mice) or 10^6 cells/well (for *Apc*$^{\Delta 716}$ and *Apc*$^{\Delta 716}$ *Stat3*$^{\Delta IEC}$ mice) to each well of 48-well plate. The respective passage experiments were performed three times, and the mean organoid numbers were counted. For the rescue experiments, 10 μM ROCK inhibitor (Y-27632; Wako, Osaka, Japan) and 5 μM GSK3 inhibitor (CHIR-99021; Tocris Bioscience, Bristol, UK) were added, and the total numbers of organoids derived from about 300 crypts were counted under a dissection microscope. Rescue experiments for each inhibitor combination were performed three times, and the mean organoid numbers were counted. For the activation of Wnt signaling, conditioned medium including afamin-associated Wnt3a (AFM-Wnt3a) was obtained from Dr. Toshiro Sato (Keio University, Japan) using a cell line established by Dr. Junichi Takagi (Osaka University, Japan) and added to the medium (27). The organoid cell proliferation was examined using the Click-iT EdU Imaging System (Invitrogen), and the EdU labeling index was calculated by counting the number of positive cells in at least five organoids. Organoids were treated with FAK inhibitor 14 (Merck, Darmstadt, Germany) at 15 μM.

Histology and immunohistochemistry

The tissue specimens were fixed in 4% paraformaldehyde, paraffin-embedded, and cut into 4-μm-thick sections. Crypts were isolated by ethylenediaminetetraacetic acid (EDTA), and organoids were fixed in 4% paraformaldehyde and embedded in iPGell (Genostaff, Tokyo, Japan). The sections were stained with H&E. For immunohistochemistry, antibodies against Ki67 (Life Technologies, Grand Island, NY, USA), CD44s (Merck, Darmstadt, Germany), phosphorylated Stat3 at Tyr705 (Cell Signaling, Danvers, MA, USA) and phosphorylated FAK at Tyr397 (Cell Signaling) were used as the primary antibodies. Staining signals were visualized using a Vectastain Elite Kit (Vector Laboratories, Burlingame, CA, USA). Apoptosis was examined using an Apoptag Peroxidase *In Situ* Apoptosis Detection Kit (Merck).

Cell culture and transplantation experiments

A mouse metastatic intestinal cancer cell line (AKTP) was established as recently described (28). AKTP cells carry $Apc^{\Delta 716}$ $Kras^{G12D}$ $Tgfbr2^{-/-}$ $Trp53^{R270H}$ mutations. To disrupt the *Stat3* gene in AKTP cells, *Stat3*-specific sgRNA was cloned into the px330 expression vector (Addgene), which bicistronically expresses sgRNA and Cas9 nuclease, and transfected to AKTP cells. The sgRNA sequence was determined by the CRSPR Design Tool (http://crispr.mit.edu/). Disruption of the *Stat3* gene was confirmed by Western blotting using a Stat3 antibody (Cell Signaling). Cell proliferation was examined using a Cell Titer-Glo 2.0 Assay (Promega Corporation, Madison, WI, USA).

For the metastasis analysis, 1×10^6 cells were transplanted into the spleen of immunodeficient NOD/Shi-*scid Il2rg*-/- mice (NSG mice; CIEA, Kanagawa, Japan) (n=3 for

each cell line), and metastatic liver lesions were examined histologically at 4 weeks after transplantation. The efficiency of metastasis was scored by the measurement of the areas of metastasized foci per total liver on H&E-stained sections.

Expression analyses

Total RNA was extracted from isolated crypts using an RNeasy Plus Micro extraction kit (Qiagen GmbH, Hilden, Germany). An expression analysis was performed using the RT^2 Profiler PCR Array (Mouse Cell Junction Pathway Finder).

Real-time reverse transcription (RT)-polymerase chain reaction (PCR)

For the real-time RT-PCR, total RNA was extracted from isolated crypts or organoids using an RNeasy Plus Micro extraction kit (Qiagen GmbH, Hilden, Germany), reverse-transcribed using a PrimeScript RT reagent kit (Takara, Tokyo, Japan), and amplified using ExTaqII SYBR Premix (Takara) on a Stratagene Mx3000P real-time thermocycler (Agilent Technologies, Santa Clara, CA, USA). The purchased primer sequences were as follows: *Itga5*-F:GAAGCTCTGAAGATGCCCTACCA, *Itga5*-R: TGATGATCCACAACGGGACAC; and *Itga6*-F:GTCACCGCTGCTGCTCAGAATA, *Itga6*-R:AGCATCAGAATCCCGGCAAG (TaKaRa, Shiga, Japan).

Statistical analyses

The data were analyzed using an unpaired *t*-test and are presented as the mean ± standard deviation (*s.d.*). *P* values of < 0.05 were considered to indicate statistical significance.

RESULTS

Stat3 is required for the regeneration of the intestinal mucosa

The epithelial Stat3 expression has been shown to be required for the regeneration of the damaged intestinal mucosa (17, 29, 30). We confirmed that phosphorylated Stat3 (P-Stat3) was detected in the cryptic cells of the X-ray-irradiated wild-type mouse intestine, while P-Stat3 in the normal intestinal epithelia was below the detection limit (Fig. 1*A*). These results indicate that the Stat3 activation is significantly increased in epithelial cells of regenerating mucosa. We then constructed *Stat3*$^{\Delta IEC}$ mice, in which Stat3 was disrupted in the intestinal epithelial cells in a cell-specific manner by the treatment of *villin-CreER Stat3*$^{flox/flox}$ mice with tamoxifen. We confirmed that P-Stat3 was not detected in the X-ray-irradiated *Stat3*$^{\Delta IEC}$ mouse intestine (Fig. 1*A*). X-ray irradiation caused a more severe phenotype in *Stat3*$^{\Delta IEC}$ mice than in wild-type mice; the 7-day survival rates of wild-type and *Stat3*$^{\Delta IEC}$ mice were 67% and 17%, respectively (Fig. 1*B*). Histologically, mucosal regeneration was significantly suppressed in *Stat3*$^{\Delta IEC}$ mice, and the number of remaining crypts at three days after irradiation in *Stat3*$^{\Delta IEC}$ mice was significantly decreased in comparison to wild-type mice (Fig. 1*C, D*). The numbers of Ki-67-positive proliferating cells and CD44-positive undifferentiated cells in the residual crypts were also significantly decreased in the *Stat3*$^{\Delta IEC}$ intestinal mucosa. These results indicate that the activation of epithelial Stat3 is required for crypt repopulation via the survival and proliferation of the residual stem cells in the damaged mucosa, which leads to regeneration.

Stat3 is required for intestinal organoid formation

To understand the biological mechanism of Stat3 in the regeneration of the intestinal mucosa, we next examined the *in vitro* organoid formation of intestinal epithelial cells, which mimics

crypt regeneration *in vivo*. Intestinal cryptic cells isolated from wild-type mice formed organoids through the construction of mini-crypt structures in Matrigel (Fig. 2*A*). Importantly, however, intestinal cryptic cells derived from *Stat3*$^{\Delta IEC}$ mice failed to generate organoids in Matrigel. Consistently, previous reports indicated that exogenous IL-22 signaling promotes organoid formation and mucosal regeneration through the induction of Stat3 activation (30, 31). Taken together, these results indicate that Stat3 activation is required for intestinal crypt reconstruction.

Next, we treated isolated cryptic cells from *Stat3*$^{\Delta IEC}$ mice with Rho-associated protein kinase (ROCK) inhibitor (Y-27632) and glycogen synthase kinase 3 (GSK3) inhibitor (CHIR-99021), as these inhibitors increase the efficiency of organoid formation through the suppression of anoikis and the activation of Wnt signaling, respectively (32). Notably, the addition of both inhibitors significantly increased the number of *Stat3*$^{\Delta IEC}$ mouse-derived organoids, while treatment with Y-27632 or CHIR-99021 alone was not sufficient for organoid recovery (Fig. 2*A*, *B*). We confirmed the disruption of *Stat3* in the rescued organoids by Western blotting, which ruled out the possibility of contamination of *Stat3* wild-type cells (Supplementary Fig. 1).

Intriguingly, once the organoids were generated from *Stat3*$^{\Delta IEC}$ intestinal crypts in the presence of inhibitors, the rescued *Stat3*$^{\Delta IEC}$ organoids no longer required inhibitor treatment for further growth (Fig. 2*C*). The organoid-forming efficiency of *Stat3*$^{\Delta IEC}$ epithelial cells was unaltered compared with wild-type after mechanical passage. Furthermore, the EdU labeling efficiency of the rescued and mechanically passaged *Stat3*$^{\Delta IEC}$ organoids was similar to that of wild-type mouse-derived organoids (Fig. 2*D*). In contrast, the development of *Stat3*$^{\Delta IEC}$ organoids was significantly suppressed when the rescued organoids were passaged after

enzymatic dissociation by trypsin (Fig. 2*E*). These results suggest that Stat3 is required for crypt formation from the remnant stem cells in the damaged mucosa due to protection from anoikis, whereas Stat3 is no longer required for the maintenance and growth of the established crypts. It is noteworthy that the conditional *Stat3* disruption in the intestinal epithelial cells of adult mice did not change the mucosal morphology, proliferation rate or differentiation into lysozymes or Muc2-expressing cells (Supplementary Fig. 2). Furthermore, the numbers of SOX7-positve undifferentiated cells in the *Stat3*$^{\Delta IEC}$ mice were similar to those in wild-type mice. These results support the idea that Stat3 is only necessary to generate new crypts from the remnant stem cells following radiation injury.

Wnt activation compensates for *Stat3* disruption to support organoid formation

It has been shown that GSK3 inhibitor increases the colony formation efficiency of intestinal stem cells through Wnt signaling activation (32,33). Since treatment with CHIR99021 is required for the recovery of *Stat3*$^{\Delta IEC}$ organoids, it is possible that Wnt signaling activation is involved in the recovery of *Stat3*$^{\Delta IEC}$ organoid formation. To assess this possibility, we cultured *Stat3*$^{\Delta IEC}$ mouse intestinal crypts in medium supplemented with the active water-soluble form of lipidated Wnt3a, which is associated with bovine serum protein afamin (AFM-Wnt3a) (27). As expected, AFM-Wnt3a treatment increased the number and size of the organoids derived from wild-type mouse crypts in comparison to organoid cultures with control medium, which is consistent with the findings of a previous report in human intestinal organoids (27) (Fig. 3*A*). Importantly, AFM-Wnt3a treatment rescued the organoid formation of *Stat3*$^{\Delta IEC}$ mouse intestinal crypts, even in the absence of an inhibitor (Fig. 3*B*). These results indicate that Wnt signaling activation can compensate for *Stat3* disruption to support the survival and

proliferation of isolated intestinal cryptic cells.

We further examined whether or not Stat3 was required for organoid formation by Wnt signaling-activated epithelial cells using a different mouse model. Adenoma cells were isolated from the intestinal polyps of *Apc*$^{\Delta 716}$ mice and *Apc*$^{\Delta 716}$ *Stat3*$^{\Delta IEC}$ compound mice and cultured in Matrigel. In these tumor cells, Wnt/β-catenin signaling is constitutively activated because of an *Apc* mutation (22). When tumor cell organoids were mechanically passaged by pipetting, the organoids developed at the same level in both genotypes, similar to normal intestine-derived organoids (Fig. 3*C*). Notably, after the enzymatic dissociation of organoids by trypsin, *Apc*$^{\Delta 716}$ *Stat3*$^{\Delta IEC}$ tumor cells formed organoids that were similar in total number and size distribution to simple *Apc*$^{\Delta 716}$ tumor-derived organoids. Taken together, these results indicate that Wnt signaling activation compensates for *Stat3* disruption to support the survival and proliferation of the dissociated normal and tumor epithelial cells through protection from anoikis.

Stat3 is dispensable for Wnt activation-driven intestinal tumorigenesis

These results prompted us to examine the role of Stat3 in the Wnt activation-driven intestinal tumorigenesis by *Apc* mutations. We examined the phenotypes of *Apc*$^{\Delta 716}$ *Stat3*$^{\Delta IEC}$ mice and age-matched simple *Apc*$^{\Delta 716}$ mutant mice. P-Stat3 was detected in the nuclei of the tumor cells of *Apc*$^{\Delta 716}$ mouse polyps but not in *Apc*$^{\Delta 716}$ *Stat3*$^{\Delta IEC}$ mice, indicating that Stat3 is activated in the Wnt-driven sporadic tumor cells (Fig. 4*A*). However, there was no significant difference in the total number of tumors between *Apc*$^{\Delta 716}$ and *Apc*$^{\Delta 716}$ *Stat3*$^{\Delta IEC}$ mice (Fig. 4*B*). The size distributions of the tumors and the number of Ki67-positive cells were also similar, and no significant difference was found in *Apc*$^{\Delta 716}$ *Stat3*$^{\Delta IEC}$ mice. These results indicate that Stat3 is

dispensable for Wnt activation-driven intestinal tumorigenesis.

Submucosal invasion was found in approximately 36% of intestinal polyps of >1 mm in size in the *Apc*$^{\Delta 716}$ *Stat3*$^{\Delta IEC}$ mice, while invasion was not found in simple *Apc*$^{\Delta 716}$ mice (Supplementary Fig. 3*A* and *B*), which is consistent with the previous findings in *Apc*^{Min} mice (12,13). We confirmed that the invasion frequency was significantly different between *Apc*$^{\Delta 716}$ mice and *Apc*$^{\Delta 716}$ *Stat3*$^{\Delta IEC}$ mice (Supplementary Fig. 3*C*). These results suggest a tumor suppressor role of Stat3; however, further investigations will be needed to confirm this point.

Next, we introduced the *Stat3*$^{\Delta IEC}$ allele into *Apc*$^{\Delta 716}$ *Tgfbr2*$^{\Delta IEC}$ compound mice, which develop invasive adenocarcinomas due to a combination of Wnt activation and TGF-β suppression (34). Notably, nuclear-accumulated P-Stat3 was detected in the tumor cells and stromal cells at the invasion front of *Apc*$^{\Delta 716}$ *Tgfbr2*$^{\Delta IEC}$ mouse tumors, whereas it was detected only in the stroma cells of *Apc*$^{\Delta 716}$ *Tgfbr2*$^{\Delta IEC}$ *Stat3*$^{\Delta IEC}$ tumors (Fig. 4*C*). However, the total number of intestinal tumors and submucosal invasion efficiency in *Apc*$^{\Delta 716}$ *Tgfbr2*$^{\Delta IEC}$ and *Apc*$^{\Delta 716}$ *Tgfbr2*$^{\Delta IEC}$ *Stat3*$^{\Delta IEC}$ mice did not differ to a statistically significant extent (Fig. 4*D*), indicating that Stat3 is not required for the submucosal invasion of intestinal tumor cells.

Stat3 is dispensable in Wnt activation-associated intestinal tumor metastasis

We recently established tumor-derived organoid cells (AKTP cells) from the intestinal tumors of *Apc*$^{\Delta 716}$ *Kras*^{G12D} *Tgfbr2*$^{-/-}$ *Trp53*^{R279H} quadruple compound mice (28). AKTP cells efficiently metastasized to the liver when transplanted into the mouse spleen. To examine whether or not Stat3 is involved in the metastatic process of Wnt-activated CRC cells, we disrupted the *Stat3* gene in AKTP cells using the CRISPR/Cas9 system (Fig. 5*A*). The disruption of *Stat3* did not significantly change the cell proliferation rate of AKTP cells (Fig.

5*B*). Furthermore, multiple metastatic foci were developed in the livers of mice after the injection of two independent lines of *Stat3*-disrupted AKTP cells into the spleen (Stat3 KO#1 and Stat3 KO#2), and the multiplicity did not differ from that of control AKTP cells to a statistically significant extent (p=0.158 and 0.201 for control vs KO#1 and KO#2, respectively) (Fig. 5*C*). Moreover, there was no significant difference in the size distributions of metastatic foci between control AKTP cells and Stat3 KO#1 or Stat3KO#2 cells. Histologically, we confirmed that Stat3 is phosphorylated in metastasized AKTP tumor cells but not in Stat3 KO cells; however, the Ki67 labeling efficiency of the *Stat3*-disrupted AKTP cells did not differ from that of control metastasized tumor cells (Fig. 5*D*). Furthermore, the expression level of total and active form β-catenin in Stat3-disrupted cells was similar to that of control AKTP cells, indicating that Wnt signaling activation is not affected by *Stat3* gene disruption (Supplementary Fig. 4). These results indicate that Stat3 is not required for metastasis of Wnt activation-associated CRC cells.

Stat3-induced integrin expression is associated with FAK activation in crypts

When intestinal crypts were isolated by EDTA treatment, we realized that $Stat3^{\Delta IEC}$ mouse-derived crypts showed a distinct morphology from the clear cylinder-like structure of wild-type crypts (Fig. 6*A*, *top*). We therefore examined the histology of isolated crypts that were collected from the intestine of wild-type and $Stat3^{\Delta IEC}$ mice by EDTA treatment for 30 min. Notably, epithelial cell alignment was impaired, and apoptosis was induced in the isolated $Stat3^{\Delta IEC}$ crypts, while the alignment of columnar epithelial cells with the lateral expression of E-cadherin was confirmed in the wild-type crypts (Fig. 6*A*). These results indicate that Stat3 is important for the survival of cryptic cells after isolation from intestine following detachment

from the extracellular matrix (ECM).

We therefore examined the changes in the expression of cell adhesion molecules using a PCR array. Notably, the expression of *Gjb1*, *Gjb2* and *Gjb3*, which encode the gap junction proteins connexin 32, 26 and 31, respectively, and *Itga5* and *Itga6*, which encode integrins α5 and α6, respectively, was significantly downregulated in the isolated *Stat3*$^{\Delta IEC}$ crypts (Fig. 6*B*). We confirmed that the expression of *Itga5* and *Itga6* was significantly decreased in the isolated *Stat3*$^{\Delta IEC}$ mouse intestinal crypts but not in the inhibitor-rescued *Stat3*$^{\Delta IEC}$ organoids by RT-PCR (Fig. 6*C*). Integrin α5 and α6 bind integrin β1 to form receptor complexes for fibronectin and laminin, respectively. It has been shown that the signaling of these ECM components through integrin complexes is important for the survival of epithelial cells through their activation of FAK, which protects cells from anoikis after detachment from the ECM (35). Importantly, phosphorylated FAK (P-FAK) was detected by immunostaining in epithelial cells of wild-type mouse-derived crypts; however, the staining intensity for P-FAK was significantly decreased in the *Stat3*$^{\Delta IEC}$ mouse-derived cryptic cells (Fig. 6*D*). To examine whether or not FAK signaling is indeed required for the organoid formation of the isolated crypts, we treated cultured organoids derived from wild-type crypts and inhibitor-rescued *Stat3*$^{\Delta IEC}$ organoids with FAK inhibitor. Of note, FAK inhibition significantly suppressed organoid development in both genotypes (Fig. 6*E*, *F*). Taken together, these results indicate that Stat3 prevents anoikis of the isolated crypts that are detached from the ECM by inducing the expression of integrin, which is associated with the activation of the FAK pathway.

DISCUSSION

It has been shown that Stat3 is required for regeneration of the damaged intestinal mucosa (17,23). We confirmed the role of Stat3 in intestinal regeneration as well as organoid formation in Matrigel, which mimics crypt formation *in vitro*. Importantly, however, we showed that Stat3 is not required for the growth of established organoids and that organoids can be maintained indefinitely by mechanical dissociation in the absence of Stat3. In contrast, *Stat3*-disrupted organoid cells were unable to survive when organoids were enzymatically dissociated by trypsin. These results indicate that while Stat3 is important in the protection of intestinal epithelial cells from acute injury and the subsequent induction of anoikis, it is not required for the maintenance and proliferation of steady-state cryptic cells (Fig. 7).

One possible mechanism underlying the impaired survival of $Stat3^{\Delta IEC}$ epithelial cells after tissue damage or crypt isolation is the downregulation of integrin α5 and α6, which complex with integrin β1 to form the receptors for fibronectin and laminin, respectively. It has been shown that integrin signaling from ECM activates FAK, which is important for the survival of epithelial cells through the further activation of the PI3K/Akt and Ras/MEK signaling pathways (35). It has also been shown that signaling through α5β1 integrin protects the intestinal epithelial cells from apoptosis (36). Thus, Stat3-dependent integrin signaling may contribute to the survival of epithelial cells through the activation of FAK signaling.

Importantly, we showed that Wnt signaling activation by an exogenous ligand compensated for *Stat3* disruption to support organoid development. It has been shown that c-Myc-induced FAK activation is required for mucosal regeneration downstream of the Wnt signaling pathway (20). It has also been shown that treatment of Apc^{Min} mice with FAK inhibitor significantly suppressed intestinal polyposis (37). Accordingly, it is possible that the

Stat3 pathway and Wnt signaling cooperatively regulate the survival of the epithelial cells in the damaged mucosa and isolated crypts through the activation of integrin/FAK signaling. It was recently shown that subepithelial telocytes are a source of Wnt ligands for intestinal epithelial cells (38). It is therefore possible that such a stromal network lining the intestinal crypts in lamina propria is disrupted in the damaged intestinal mucosa, resulting in a decrease in Wnt signaling activity in regenerating epithelial cells, which may impair the stem cell properties of the residual stem cells. Under such Wnt-suppressed circumstances, Stat3 is important for the survival of epithelial cells through the activation of FAK signaling. In contrast, when Wnt signaling is sufficiently activated, Stat3 is not required for the survival of epithelial cells (Fig. 7). This hypothesis may explain why Wnt activation-driven tumor cells do not require Stat3 activation.

It has been shown that Paneth cells generate a stem cell niche through Wnt ligand secretion (39), and IL-6-induced Stat3 activation in Paneth cells increases organoid cell proliferation through Wnt activation (40). Accordingly, it is also possible that suppression of Paneth cell-dependent Wnt signaling causes impaired regeneration and crypt formation in *Stat3*$^{\Delta IEC}$ mice.

With regard to the role of Stat3 in tumorigenesis, it has been shown that the blocking of IL-6 and IL-11 cytokine signaling or downstream transcription factor Stat3 causes the significant suppression of CAC development in mouse models, indicating that Stat3 is indispensable for inflammation-associated colonic tumorigenesis (8-10). However, we showed in the present study that Stat3 was not required for intestinal tumor development in *Apc*$^{\Delta 716}$ mice and that submucosal invasion was not suppressed in *Apc*$^{\Delta 716}$ *Tgfbr2*$^{\Delta IEC}$ mice by Stat3 disruption. Furthermore, Stat3 is also dispensable for liver metastasis of *Apc*$^{\Delta 716}$ *Kras*^{G12D}

Tgfbr2$^{-/-}$ *Trp53*^{R270H} tumor cells. These genetic results indicate that Stat3 does not play an important role in Wnt activation-driven colonic tumorigenesis or the malignant progression of CRC (Fig. 7); thus, its role differs from that in CAC development. Accordingly, in CAC development, it is possible that Stat3 is required for the survival and proliferation of tumor cells initiated in the ulcerative colitis mucosa, similarly to normal epithelial cells. In contrast, in sporadic CRC development, Wnt signaling is constitutively activated by the genetic alteration of *APC* or *CTNNB1*, which is sufficient to support the survival of tumor cells independently of the Stat3 pathway. In the present study, we showed that the epithelial Stat3 pathway is not required for Wnt-driven tumorigenesis; however, Stat3 in stromal cells is also activated in the inflammatory microenvironment of intestinal tumors. Thus, it is still possible that stromal Stat3 plays a role in sporadic tumorigenesis.

We also found that Stat3 disruption induced the submucosal invasion of intestinal tumors of *Apc*$^{\Delta 716}$ mice, which is consistent with the findings of previous reports using *Apc*^{Min} *Stat3*-/- compound mice (12,13). It has also been shown that Stat3 suppresses KRAS-induced lung tumorigenesis and p19^{ARF} expression-associated prostate cancer metastasis (41, 42). Thus, Stat3 may play a tumor suppressor role in the malignant progression of CRC. However, a further analysis to compare the results of mouse experiments and human CRC findings is needed to draw hard conclusions in this regard.

In conclusion, Stat3 is required for the survival and proliferation of the remaining epithelial cells in the damaged mucosa; thus, Stat3 is indispensable for mucosal regeneration and CAC development. In contrast, Stat3 is not required for Wnt activation-driven tumor development or the malignant progression of CRC (Fig. 7). Mechanistically, Wnt signaling and Stat3 cooperate to support the survival of cryptic epithelial cells through the activation of the

integrin/FAK signaling pathway, which protects epithelial cells from anoikis. When Wnt signaling is sufficiently activated, Stat3 is no longer required for the survival or proliferation of normal and tumor epithelial cells. Thus, the degree of Wnt activation in cancer cells has an important impact on the efficacy of Stat3 inhibitor treatment in CRC patients.

ACKNOWLEDGEMENTS

We thank Manami Watanabe, Ayako Tsuda and Yoshie Jomen for their technical assistance. This study was supported by AMED-CREST (JP17gm0410014) and AMED (JP17ck0106259), Japan Agency for Medical Research and Development, Japan; and Grants-in-Aid for Scientific Research (A) (JP18H04030) and (C) (JP16K07111) from the Ministry of Education, Culture, Sports, Science and Technology of Japan; Takeda Science Foundation; and Mitsubishi Foundation. The authors declare no conflicts of interest.

AUTHOR CONTRIBUTIONS

H. Oshima, D.C. Voon, and M. Oshima designed the study; H. Oshima, S.Y. Kok performed the study; M. Nakayama and K. Murakami provided resources and analytic tools; M. Oshima wrote the manuscript; all authors discussed the results and edited the final manuscript.

REFERENCES

1. Grivennikov, S.I., Greten, F.R., and Karin, M. (2010) Immunity, inflammation, and cancer. *Cell* **140**, 883-899
2. He, G., and Karin, M. (2011) NF-κB and STAT3-key players in liver inflammation and cancer. *Cell Res.* **21**, 159-168
3. Frank, D.A. (2007) STAT3 as a central mediator of neoplastic cellular transformation. *Cancer Lett*. **251**, 199-210
4. Roeser, J.C., Leach, S.D., and McAllister, F. (2015) Emerging strategies for cancer immunoprevention. *Oncogene* **34**, 6029-6039
5. Kusaba, T., Nakayama, T., Yamazumi, K., Yakata, Y., Yoshizaki, A., Nagayasu, T., and Sekine, I. (2005) Expression of p-STAT3 in human colorectal adenocarcinoma and adenoma; correlation with clinicopathological factors. *J. Clin. Pathol.* **58**, 833-838
6. Corvinus, F.M., Orth, C., Moriggl, R., Tsareva, S.A., Wagner, S., Pfitzner, E.B., Baus, D., Kaufmann, R., Huber, L.A., Zatloukal, K. Beug, H., Ohlschlager, P, Schutz, A, Halbhuber, K.-J., and Friedrich, K. (2005) Persistent STAT3 activation in colon cancer is associated with enhanced cell proliferation and tumor growth. *Neoplasia* **7**, 545-555
7. Lin, L., Liu, A., Peng, Z., Lin, H.-J., Li, P.-K., Li, C. and Lin, L. (2011) STAT3 is necessary for proliferation and survival in colon cancer-initiating cells. *Cancer Res.* **71**, 7226-7237
8. Bollrath, J., Phesse, T.J., von Burstin, V.A., Putoczki, T., Bennecke, M., Bateman, T., Nebelsiek, T., Lundgren-May, T., Canli, O., Schwitalla, S., Matthews, V., Schmid, R.M., Kirchner, T., Arkan, M.C., Ernst, M., and Greten, F.R. (2009) gp130-mediated Stat3 activation in enterocytes regulates cell survival and cell-cycle progression during colitis-associated tumorigenesis. *Cancer Cell* **15**, 91-102

9. Grivennikov, S., Karin, E., Terzic, J., Mucida, D., Yu, G.-Y., Vallabhapurapu, S., Scheller, J., Rose-John, S., Cheroutre, H., Eckmann, L, and Karin, M. (2009) IL-6 and Stat3 are required for survival of intestinal epithelial cells and development of colitis-associated cancer. *Cancer Cell* **15**, 103-113
10. Putoczki, T.L., Thiem, S., Loving, A., Busuttil, R.A., Wilson, N.J., Ziegler, P.K., Nguyen, P.M., Preaudet, A., Farid, R., Edwards, K.M., Boglev, Y., Luwor, R.B., Jarnicki, A., Horst, D., Boussioutas, A., Heath, J.K., Sieber, O.M., Pleines, I., Kile, B.T., Nash, A., Greten, F.R., McKenzie, B.S., and Ernst, M. (2013) Interleukin-11 is the dominant IL-6 family cytokine during gastrointestinal tumorigenesis and can be targeted therapeutically. *Cancer Cell* **24**, 257-271
11. Johnson, D.E., O'Keefe, R.A., and Grandis, J.R. (2018) Targeting the IL-6/JAK/STAT3 signalling axis in cancer. *Nat Rev Clin Oncol* **15**, 234-248
12. Musteanu, M., Blaas, L., Mair, M., Schlederer, M., Bilban, M., Tauber, S., Esterbauer, H., Mueller, M., Casanova, E., Kenner, L., Poli, V., and Eferi, R. (2010) Stat3 is a negative regulator of intestinal tumor progression in *Apc*^{Min} mice. *Gastroenterology* **138**, 1003-1011
13. Lee, J., Kim, J.C.K., Lee, S.E., Quinley, C., Kim, H.R., Herdman, S., Corr, M., and Raz, E. (2012) Signal transducer and activator of transcription 3 (STAT3) protein suppresses adenoma-to-carcinoma transition in *Apc*$^{min/+}$ mice via regulation of Snail-1 (SNAI) protein stability. *J Biol Chem* **287**, 18182-18189
14. The Cancer Genome Atlas Network. (2012) Comprehensive molecular characterization of human colon and rectal cancer. *Nature* **487**, 330-337
15. Matthews, J.R., Sansom, O.J., and Clarke, A.R. (2011) Absolute requirement for STAT3 function in small-intestine crypt stem cell survival. *Cell Death Differ* **18**, 1934-1943

16. Willson, T.A., Jurickova, I., Collins, M., and Denson, L.A. (2013) Deletion of intestinal epithelial cell STAT3 promotes T-lymphocyte STAT3 activation and chronic colitis following acute dextran sodium sulfate injury in mice. *Inflamm Bowel Dis* **19**, 512-525
17. Phesse, T.J., Buchert, M., Stuart, E., Flanagan, D.J., Faux, M., Afshar-Sterle, S., Walker, F., Zhang H. H., Nowell, C.J., Jorissen, R., Tan, C.W., Hirokawa, Y., Eissmann, M.F., Poh, A.R., Malaterre, J., Pearson, H.B., Kirsh, D.G., Provero, P., Poli, V., Ramsay, R.G., Sieber, O., Burgess, A.W., Huszar, D., Vincan, E., and Ernst, M. (2014) Partial inhibition of gp130-Jak-Stat3 signaling prevents Wnt-β-catenin-mediated intestinal tumor growth and regeneration. *Sci Sig* **7**, ra92
18. Krausova, M., and Korinek, V. (2014) Wnt signaling in adult intestinal stem cells and cancer. *Cell Sig* **26**, 570-509
19. Nusse, R., and Clevers, H. (2017) Wnt/β-catenin signaling, disease, and emerging therapeutic modalities. *Cell* **169**, 985-999
20. Ashton, G.H., Morton, J.P., Myant, K., Phesse, T.J., Ridgway, R.A., Marsh, V. Wikins, J.A., Athineos, D., Muncan, V., Kemp, R., Neufeld, K., Clevers, H., Brunton, V., Winton, D.J., Wang, X., Sears, R.C., Clarke, A.R., Frame, M.C., and Sansom, O.J. (2010) Focal adhesion kinase is required for intestinal regeneration and tumorigenesis downstream of Wnt/c-Myc signaling. *Dev Cell* **19**, 259-269
21. Oudhoff, M.J., Braam, M.J.S., Freeman, S.A., Wong, D., Rattray, D.G., Wang, J., Antignano, F., Snyder, K., Refaeli, I., Hughes, M.R., McNagny, K.M., Gold, M.R., Arrowsmith, C.H., Sato, T., Rossi, F.M.V.,Tatlock, J.H., Owen, D.R., Brown, P.J., and Zaph, C. (2016) SETD7 controls intestinal regeneration and tumorigenesis by regulating Wnt/β-catenin and Hippo/YAP signaling. *Dev Cell* **37**, 47-58

22. Oshima, M., Oshima, H., Kitagawa, K., Kobayashi, M., Itakura, C., and Taketo, M. (1995) Loss of Apc heterozygosity and abnormal tissue building in nascent intestinal polyps in mice carrying a truncated Apc gene. *Proc Natl Acad Sci USA* **92**, 4482-4486

23. Takeda, K., Kaisho, T., Yoshida, N., Takeda, J., Kishimoto T, and Akira S. (1998) Stat3 activation is responsible for IL-6-depenndent T cell proliferation through preventing apoptosis: generation and characterization of T cell-specific Stat3-deficient mice. *J Immunol* **161**, 4652-4660

24. el Marjou, F., Janssen, K.P., Chang, B.H., Li, M., Chan, L., Louvard, D., Chambon P., Metzger, D., and Robine, S. (2004) Tissue-specific and inducible Cre-mediated recombination in the gut epithelium. *Genesis* **39**, 186-193

25. Chytil, A., Magnunson, M.A., Wright, C.V., and Moses, H.L. (2002) Conditional inactivation of the TGF-β type II receptor using Cre:Lox. *Genesis* **32**, 73-75

26. Sato, T., Vries, R.G., Snippert, H.J., van de Wetering, M., Barker, N., Stange, D.E., van Es, J.H., Abo, A., Kujala, P., Peters, P.J., and Clevers, H. (2009) Single Lgr5 stem cells build crypt-villus structures *in vitro* without a mesenchymal niche. *Nature* **459**, 262-265

27. Mihara, E., Hirai, H., Yamamoto, H., Tamura-Kawakami, K., Matano, M., Kikuchi, A. Sato T., and Takagi J. (2016) Active and water-soluble form of lipidated Wnt protein is maintained by a serum glycoprotein afamin/α-albumin. *eLife* **5**, e11621

28. Sakai, E., Nakayama, M., Oshima, H., Kouyama, Y., Niida, A., Fujii, S., Ochiai, A., Nakayama, K.I., Mimori, K., Suzuki, Y., Hong, C.P., Ock, C.Y., Kim, S.J., and Oshima, M. (2018) Combined mutation of Apc, Kras and Tgfbr2 effectively drives metastasis of intestinal cancer. *Cancer Res* **78**, 1334-1346

29. Pickert, G., Neufert, C., Leppkes, M., Zheng, Y., Wittkopf, N., Warntjen, M., Lehr, H.A.,

Hirth, S., Weigmann, B., Wirtz, S., Ouyang, W., Neurath, M.F., and Becker, C. (2009) STAT3 links IL-22 signaling in intestinal epithelial cells to mucosal wound healing. *J Exp Med* **206**, 1465-1472

30. Lindemans, C.A., Calafiore, M., Mertelsmann, A.M., O'Connor, M.H., Dudakov, J.A., Jenq, R.R., Velardi, E., Young, L.F., Smith, O.M., Lawrence, G., Ivanov, J. A., Fu, Y.Y., Takashima, S., Hua, G., Martin, M.L., O'Rourke, K.P., Lo, Y.H., Mokry, M., Romera-Hernandez, M., Cupedo, T., Dow, L., Nieuwenhuis, E.E., Shroyer, N.F., Liu, C., Kolesnick, R., van den Brink, M.R.M., and Hanash, A.M. (2015) Interleukin-22 promotes intestinal-stem cell-mediated epithelial regeneration. *Nature* **528**, 560-564
31. Aparicio-Domingo, P., Romera-Hernandez, M., Karrich, J.J., Cornelissen, F., Papazia, N., Lindenbergh-Kortleve, D.J., Butler, J.A., Boon, L., Coles, M.C., Samsom, J.N., and Cupedo, T. (2015) Type 3 innate lymphoid cells maintain intestinal epithelial stem cells after tissue damage. *J Exp Med* **212**, 1783-1791
32. Fujii, M., Matano, M., Nanki, K., and Sato, T. (2015) Efficient genetic engineering of human intestinal organoids using electroporation. *Nat Protoc* **10**, 1474-1485
33. Wang, F., Scoville, D., He, X.C., Mahe, M.M., Box, A., Perry, J.M., Smith, N.R., Lei, N.Y., Davies, P.S., Fuller, M.K., Haug, J.S., McClain, M., Gracz, A.D., Ding, S., Stelzner, M., Dunn, J.C., Magness, S.T., Wong, M.H., Martin, M.G., Helmrath, M., and Li, L. (2013) Isolation and characterization of intestinal stem cells based on surface marker combinations and colony-formation assay. *Gastroenterology* **145**, 383-395
34. Oshima, H., Nakayama, M., Han, T.S., Naoi, K., Ju, X., Maeda, Y., Robine, S., Tsuchiya, K., Sato, T., Taketo, M.M., and Oshima, M. (2015) Suppressing TGFβ signaling in regenerating epithelia in an inflammatory microenvironment is sufficient to cause invasive

intestinal cancer. *Cancer Res* **75**, 766-776

35. Guo, W, and Giancotti, F.G. (2004) Integrin signalling during tumour progression. *Nat Rev Mol Cell Biol* **5**, 816-826
36. Lee, J.W., and Juliano, R.L. (2000) α5β1 integrin protects intestinal epithelial cells from apoptosis through a phosphatidylinositol 3-kinase and protein kinase B-dependent pathway. *Mol Biol Cell* **11**, 1973-1987
37. Gao, C., Chen, G., Kuan, S.F., Zhang, D.H., Schlaepfer, D.D., and Hu, J. (2015) FAK/PYK2 promotes the Wnt/β-catenin pathway and intestinal tumorigenesis by phosphorylating GSK3β. *Elife* **4**, e10072
38. Shoshkes-Carmel, M., Wang, Y.J., Wangensteen, K.J., Toth, B., Kondo, A., Massassa, E.E., Itzkovitz, S., and Kaestner, K.H. (2018) Subepithelial telocytes are an important source of Wnts that supports intestinal crypts. *Nature* **557**, 242-246
39. Sato, H., van Es, J.H., Snippert, H.J., Stange, D.E, Vries, R.G., van den Born, M., Barker, N., Shroyer, N.F., van de Wetering, M., and Clevers, H. (2011) Paneth cells constitute the niche for Lgr5 stem cells in intestinal crypts. *Nature* **469**, 415-418
40. Jeffery, V., Goldson, A.J., Dainty, J.R., Chieppa, M., and Sobolewski, A. (2017) IL-6 signaling regulates small intestinal crypt homeostasis. *J Immunol* **199**, 304-311
41. Grabner, B., Schramek, D., Mueller, K.M., Moll, H.P., Svinka, J., Hoffmann, T., Bauer, E., Blass, L., Hruschka, N., Zboray, K., Stiedl, P., Nivarthi, H., Bogner, E., Gruber, W., Mohr, T., Zwick, R.H., Kenner, L., Poli, V., Aberger, F., Stoiber, D., Egger, G., Esterbauer, H., Zuber, J., Moriggl, R., Eferl, R., Győrffy, B., Penninger, J.M., Popper, H., and Casanova, E. (2015) Disruption of STAT3 signalling promotes KRAS-induced lung tumorigenesis. *Nat Commun* **6**, 6285

42. Pencik, J., Schlederer, M., Gruber, W., Unger, C., Wlker, S.M., Chalaris, A., Marié, I.J., Hassler, M.R., Javaheri, T., Aksoy, O., Blayney, J.K., Prutsch, N., Skucha, A., Herac, M., Krämer, O.H., Mazal, P., Grebien, F., Egger, G., Poli, V., Mikulits, W., Eferl, R., Esterbauer, H., Kennedy, R., Fend, F., Scharpf. M., Braun, M., Perner, S., Levy, D.E., Malcolm, T., Turner, S.D., Haitel, A., Susani, M., Moazzami, A., Rose-John, S., Aberger, F., Merkel, O., Moriggl, R., Culig, Z., Dolznig, H., and Kenner, L. (2015) STAT3 regulated ARF expression suppresses prostate cancer metastasis. *Nat Commun* **6**, 7736

Figure Legends

Figure 1. The histological analysis of the X-ray-irradiated mouse small intestine. *A*) Representative sections immunohistochemically stained for phosphorylated Stat3 (P-Stat3) in the small intestine of control wild-type and irradiated wild-type and irradiated *Stat3*$^{\Delta IEC}$ mice. Bars, 100 μm. Insets indicate enlarged images of the boxed areas. *B*) The survival rate of wild-type and *Stat3*$^{\Delta IEC}$ mice after X-ray-irradiation (n=9 for wild-type and n=12 for *Stat3*$^{\Delta IEC}$ mice). *C*) Representative histology sections from wild-type (*left*) and *Stat3*$^{\Delta IEC}$ (*right*) mouse intestines (H&E) (*top*) and immunohistochemical staining for Ki67 (*middle*) and CD44 (*bottom*). Insets show enlarged image views of the boxed areas. Bars, 100 μm. *D*) The mean number of crypts in the microscopy fields (*left*) and Ki67-positive cells per crypt (*right*) are shown (mean ± *s.d.*). Asterisk, $p < 0.05$.

Figure 2. The role of Stat3 in organoid formation from intestinal crypts. *A*) A schematic illustration of tamoxifen (Tam) treatment and organoid formation (*top*). Representative microscopic photographs of organoid cultures of intestinal crypts of wild-type and *Stat3*$^{\Delta IEC}$ mice on day 2 (*left*) and day 4 (*right*). Arrowheads indicate organoids rescued by inhibitors (Y-27632 and CHIR-99021). Bars, 250 μm. *B*) The mean numbers of organoids per well developed from the intestinal crypts of wild-type (*top*) and *Stat3*$^{\Delta IEC}$ mice (*bottom*) in the indicated inhibitor conditions are shown (mean ± *s.d.*). Asterisk, $p < 0.05$; and N.S., not significant. Inhibitor treatment experiments were performed three times for each mouse genotype. *C*) A schematic illustration of organoid passaging by mechanical pipetting (*top*). Representative microscopic photographs of organoids passaged from wild-type and *Stat3*$^{\Delta IEC}$ rescued organoids (*bottom*). Insets show enlarged views. Bars, 250 μm. The mean numbers of organoids

> 150 μm are shown in the bar graph (mean ± *s.d.*). The mechanical passage experiments were performed three times. *D*) Immunohistochemical staining of wild-type (*top*) and *Stat3*$^{\Delta IEC}$ (*bottom*) rescued organoids for EdU (*green*) and E-cadherin (*red*). EdU labeling efficiency is shown in the bar graph (mean ± *s.d.*). N.S., not significant. *E*) A schematic illustration of organoid passaging by trypsin treatment (*top*). Representative microscopic photographs of organoids passaged from wild-type (*top*) and *Stat3*$^{\Delta IEC}$-rescued organoids (*bottom)*. Bars, 200 μm (day 0) and 1mm (day 10). The mean numbers of organoids are shown in the bar graph (mean ± *s.d.*). Asterisk, $p < 0.05$. The enzymatic passage experiments were performed three times.

Figure 3. Wnt activation compensates for *Stat3* disruption to support organoid formation. *A*) A schematic illustration of Tam treatment and organoid formation (*top*). Representative microscopic photographs of organoids of the intestinal crypts from wild-type mice cultured with control medium (*top*) and AFM-Wnt3a (*bottom*) on day 2 (*left*) and day 5 (*right*). Bars, 250 μm. *B*) Representative microscopic photographs of organoid cultures of the intestinal crypts from *Stat3*$^{\Delta IEC}$ mice cultured with control medium (*top*), AFM-Wnt3a without inhibitor (*middle*) and with inhibitor (bottom) on days 3 (*left*) and 5 (*right*). Bars, 250 μm. *C*) A schematic illustration of Tam treatment, tumor-derived organoid formation and treatment with pipetting or trypsin to passage (*top*). Representative microscopic photographs of the primary organoids (*left*; Bars, 250 μm) and organoids passaged by pipetting (*middle*; Bars, 250 μm) and trypsin treatment (*right*; Bars, 500 μm) derived from intestinal tumors of *Apc*$^{\Delta 716}$ simple mutant mice (*top*) and *Apc*$^{\Delta 716}$ *Stat3*$^{\Delta IEC}$ compound mice (*bottom*). The mean numbers of organoids (*top*) and size distributions (*bottom*) after passaging with trypsin treatment in the respective

genotype are shown in the bar graphs (mean ± *s.d.*). N.S., not significant. The experiments were performed three times.

Figure 4. The dispensable role of Stat3 in Wnt-driven intestinal tumorigenesis. *A*) A schematic illustration of Tam treatment of *Apc*$^{\Delta 716}$ mice (n=10) and *Apc*$^{\Delta 716}$ *villin-CreER Stat3*$^{flox/flox}$ mice (n=12) (*top*). Representative histology sections of small intestinal tumors of *Apc*$^{\Delta 716}$ mice (*left*) and *Apc*$^{\Delta 716}$ *Stat3*$^{\Delta IEC}$ mice (*right*) (H&E) (*top*) and immunohistochemical staining for Ki67 (*middle*) and phosphorylated Stat3 (P-Stat3) (*bottom*). Insets show enlarged views. Bars, 200 μm. *B*) The total numbers of polyps in each mouse are shown with dots with the mean values (*top*). The size distribution is shown in the bar graph (mean ± *s.d.*). *C*) A schematic illustration of the Tam treatment of *Apc*$^{\Delta 716}$ *villin-CreER Tgfbr2*$^{flox/flox}$ mice (n=10) and *Apc*$^{\Delta 716}$ *villin-CreER Tgfbr2*$^{flox/flox}$ *Stat3*$^{flox/flox}$ mice (n=8) (*top*). Representative histology sections of small intestinal tumor of *Apc*$^{\Delta 716}$ *Tgfbr2*$^{\Delta IEC}$ mice (*left*) and *Apc*$^{\Delta 716}$ *Tgfbr2*$^{\Delta IEC}$ *Stat3*$^{\Delta IEC}$ mice (*right*) for H&E (*top*) and immunohistochemical staining for P-Stat3 (*bottom*). Insets show enlarged views of boxed areas. Bars, 400 μm. *D*) The total numbers of polyps (*top*) and invasive polyps (bottom) per section are shown with the mean number. N.S., not significant.

Figure 5. The dispensable role of Stat3 in Wnt activation-associated cancer cell metastasis. *A*) Western blotting results for Stat3 in control AKTP cells (Cont) and Stat3-targeted AKTP cell lines, Stat3 KO #1 and #2, by CRISPR/Cas9. β-catenin was used for internal controls. *B*) The results of the cell proliferation analysis of control and Stat3 KO#1 and #2 AKTP cells (mean ± *s.d.*). *C*) Control AKTP cells (Cont) and Stat3-targeted AKTP cell lines (Stat3 KO#1 and #2) were transplanted to the spleen of NSG mice (n=3 for each cell line). Representative

macroscopic photographs of mouse livers at four weeks after spleen transplantation are shown (*top*). Arrowheads indicate metastatic foci. The mean metastasis tumor areas (*bottom left*) and size distribution of metastatic foci (*bottom right*) on the histological sections are shown in the bar graphs (mean ± *s.d.*). N.S., not significant. *D*) Representative low-powered images of liver metastasis (H&E) (*top*) and high-powered images of serial sections of metastatic foci (H&E) and immunohistochemical staining for P-Stat3 and Ki67 (from *top* to *bottom*). Dotted lines indicate metastatic foci for each genotype. Insets show enlarged views inside of metastatic foci. Bars, 200 μm.

Figure 6. The Stat3-dependent integrin expression and FAK activation. *A*) Representative photographs of isolated crypts under a dissection microscope, a histological section of isolated crypts (H&E), and immunohistochemical staining for E-cadherin and ApopTag (from *top* to *bottom*) of wild-type (*left*) and *Stat3*$^{\Delta IEC}$ isolated intestinal crypts (*right*). Insets show enlarged views. Bars, 100 μm. *B*) Results of the filter array expression analysis are shown in the dot graph, which displays the upregulated (> 4 fold) and downregulated (< 0.25 fold) genes in the *Stat3*$^{\Delta IEC}$ crypts in different colors. *C*) The relative mRNA levels in the isolated crypts (*top*) and rescued organoids (*bottom*) (mean ± *s.d.*) were examined by RT-PCR for *Itega5* and *Itega6*. Asterisk, < 0.05. *D*) Isolated crypts from wild-type (*left*) and *Stat3*$^{\Delta IEC}$ mice (*right*) that were subjected to immunohistochemical staining for phosphorylated FAK (P-FAK). Bars, 50 μm. *E*) Representative microscopic photographs of organoids derived from wild-type (*top*) and *Stat3*$^{\Delta IEC}$ mouse (*bottom*) crypts in the absence (*left*) or presence (*right*) of FAK inhibitor in the Matrigel. Insets show enlarged views. Note that crypt growth was suppressed by FAK inhibitor regardless of genotypes. Bars, 250 μm. *F*) The mean numbers of developed organoids (budding

number > 5) in the Matrigel with or without FAK inhibitor (*FAKi* and *NT*, respectively) are shown (mean ± *s.d.*). Asterisk, $p < 0.05$.

Figure 7. A schematic illustration of the role of Stat3 in regeneration and tumorigenesis of intestinal crypts. Wild-type (*top*) and $Stat3^{\Delta IEC}$ crypts (*bottom*) are shown. Stat3 is required for regeneration from damaged mucosa, which may be compensated by Wnt activation (*left*). In contrast, Stat3 is dispensable for Wnt activation-driven tumorigenesis (*right*).

Figure 1

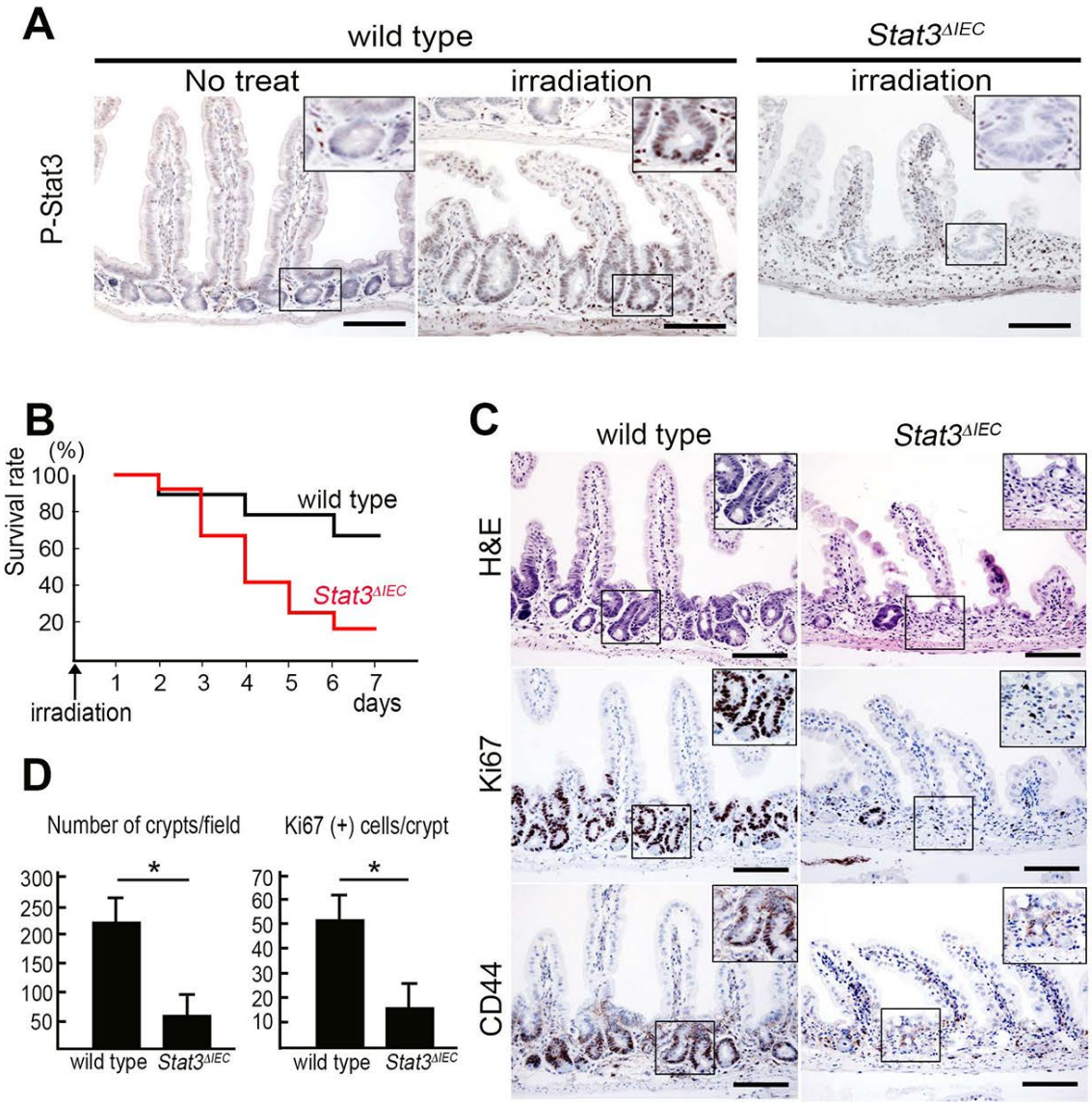
A
wild type
Stat3ΔIEC
No treat
irradiation
irradiation
P-Stat3
B
Survival rate (%)
100
80
60
40
20
wild type
Stat3ΔIEC
1 2 3 4 5 6 7
days
irradiation
C
wild type
Stat3ΔIEC
H&E
Ki67
CD44
D
Number of crypts/field
Ki67 (+) cells/crypt
300
250
200
150
100
50
70
60
50
40
30
20
10
*
*
wild type
Stat3ΔIEC
wild type
Stat3ΔIEC

Figure 2

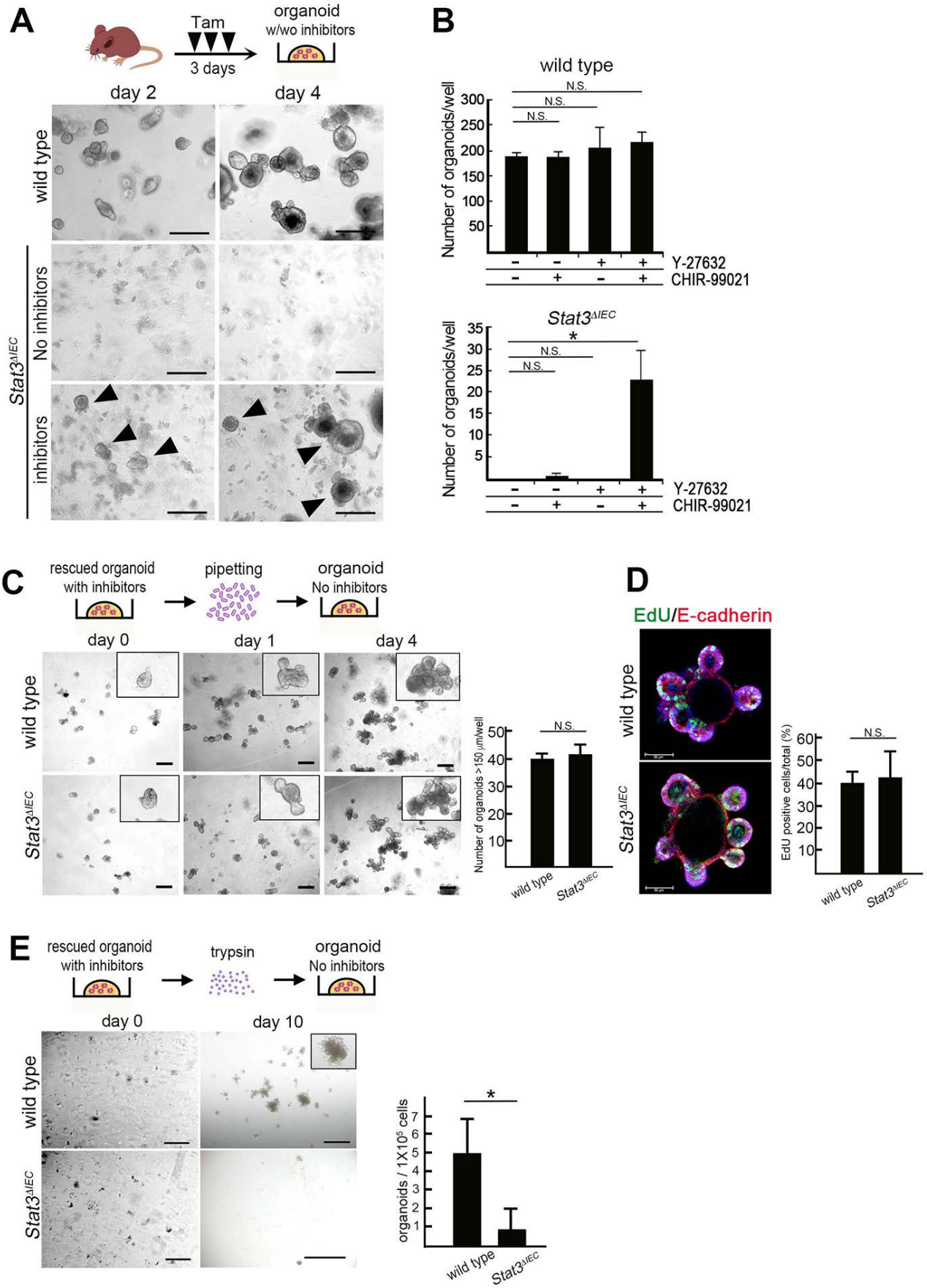
A
Tam
3 days
organoid
w/wo inhibitors
day 2
day 4
wild type
Stat3ΔIEC
No inhibitors
inhibitors
B
wild type
Number of organoids/well
N.S.
N.S.
N.S.
Y-27632
CHIR-99021
Stat3ΔIEC
*
C
rescued organoid
with inhibitors
pipetting
organoid
No inhibitors
day 0
day 1
day 4
Number of organoids >150 μm/well
D
EdU/E-cadherin
EdU positive cells/total (%)
E
rescued organoid
with inhibitors
trypsin
organoid
No inhibitors
day 0
day 10
organoids / 1X10^5 cells

Figure 3

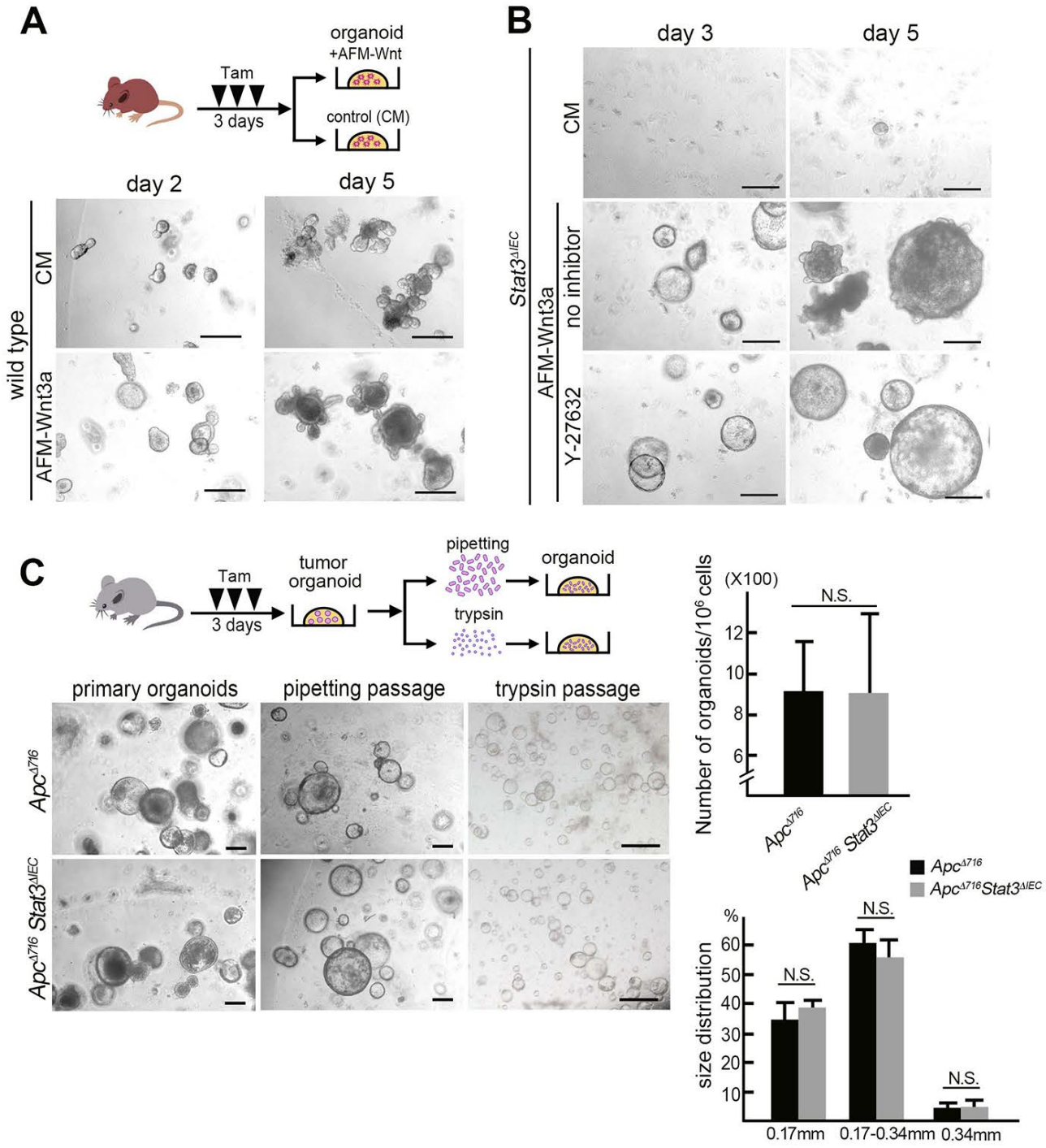
A
organoid
+AFM-Wnt
Tam
3 days
control (CM)
day 2
day 5
wild type
CM
AFM-Wnt3a
B
day 3
day 5
Stat3ΔIEC
CM
AFM-Wnt3a
no inhibtor
Y-27632
C
Tam
3 days
tumor
organoid
pipetting
organoid
trypsin
primary organoids
pipetting passage
trypsin passage
Apcᴬ716
Apcᴬ716 Stat3ΔIEC
Number of organoids/10⁶ cells
(X100)
N.S.
12
10
8
6
Apcᴬ716
Apcᴬ716 Stat3ΔIEC
Apcᴬ716
Apcᴬ716Stat3ΔIEC
%
size distribution
60
50
40
30
20
10
N.S.
N.S.
N.S.
0.17mm
0.17-0.34mm
0.34mm

Figure 4

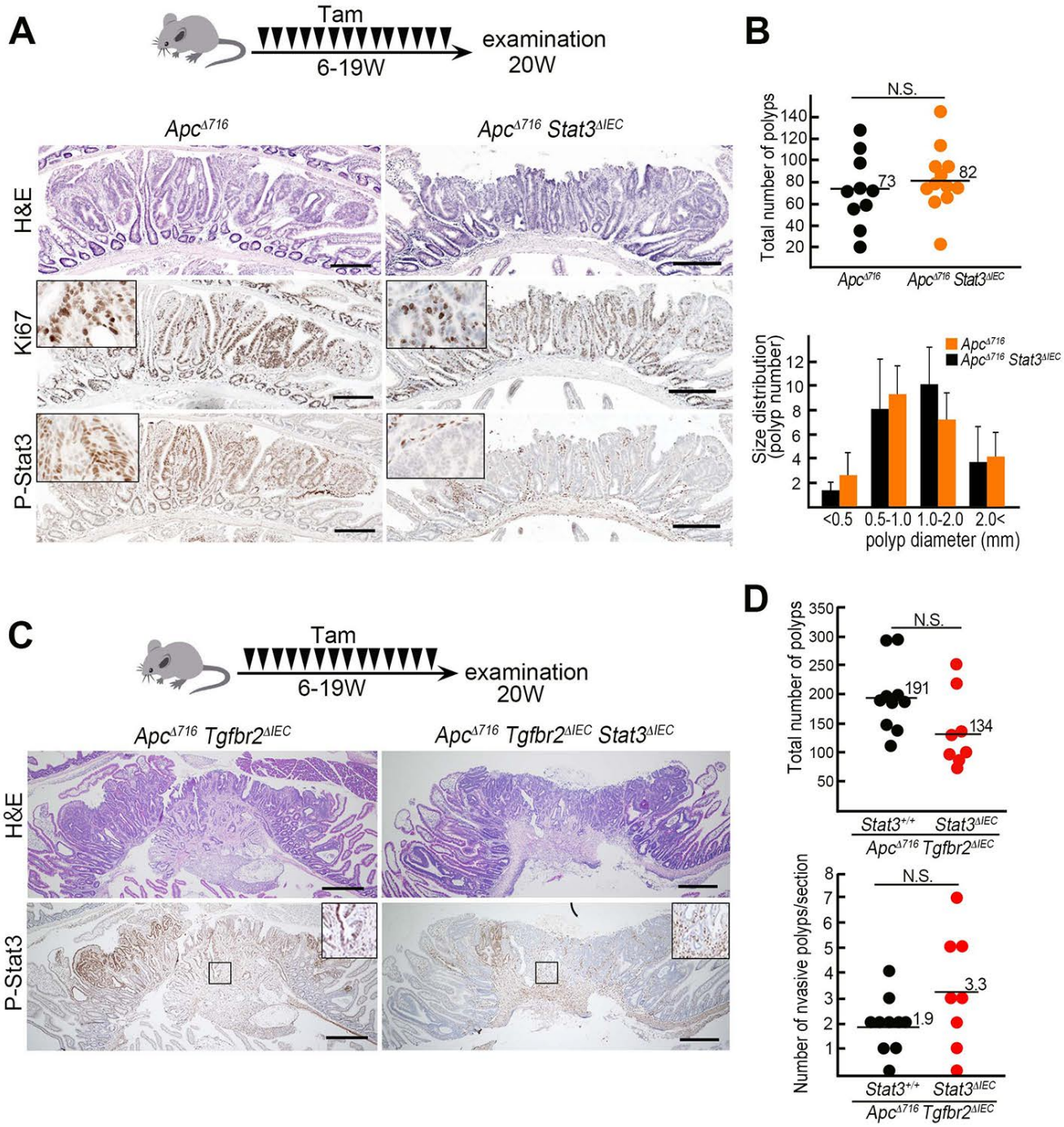
A
Tam
6-19W
examination
20W
Apc^Δ716
Apc^Δ716 Stat3^ΔIEC
H&E
Ki67
P-Stat3
B
N.S.
Total number of polyps
73
82
Apc^Δ716
Apc^Δ716 Stat3^ΔIEC
Size distribution (polyp number)
<0.5
0.5-1.0
1.0-2.0
2.0<
polyp diameter (mm)
C
Tam
6-19W
examination
20W
Apc^Δ716 Tgfbr2^ΔIEC
Apc^Δ716 Tgfbr2^ΔIEC Stat3^ΔIEC
H&E
P-Stat3
D
N.S.
Total number of polyps
191
134
Stat3^+/+
Stat3^ΔIEC
Apc^Δ716 Tgfbr2^ΔIEC
N.S.
Number of nvasive polyps/section
1.9
3.3
Stat3^+/+
Stat3^ΔIEC
Apc^Δ716 Tgfbr2^ΔIEC

Figure 5

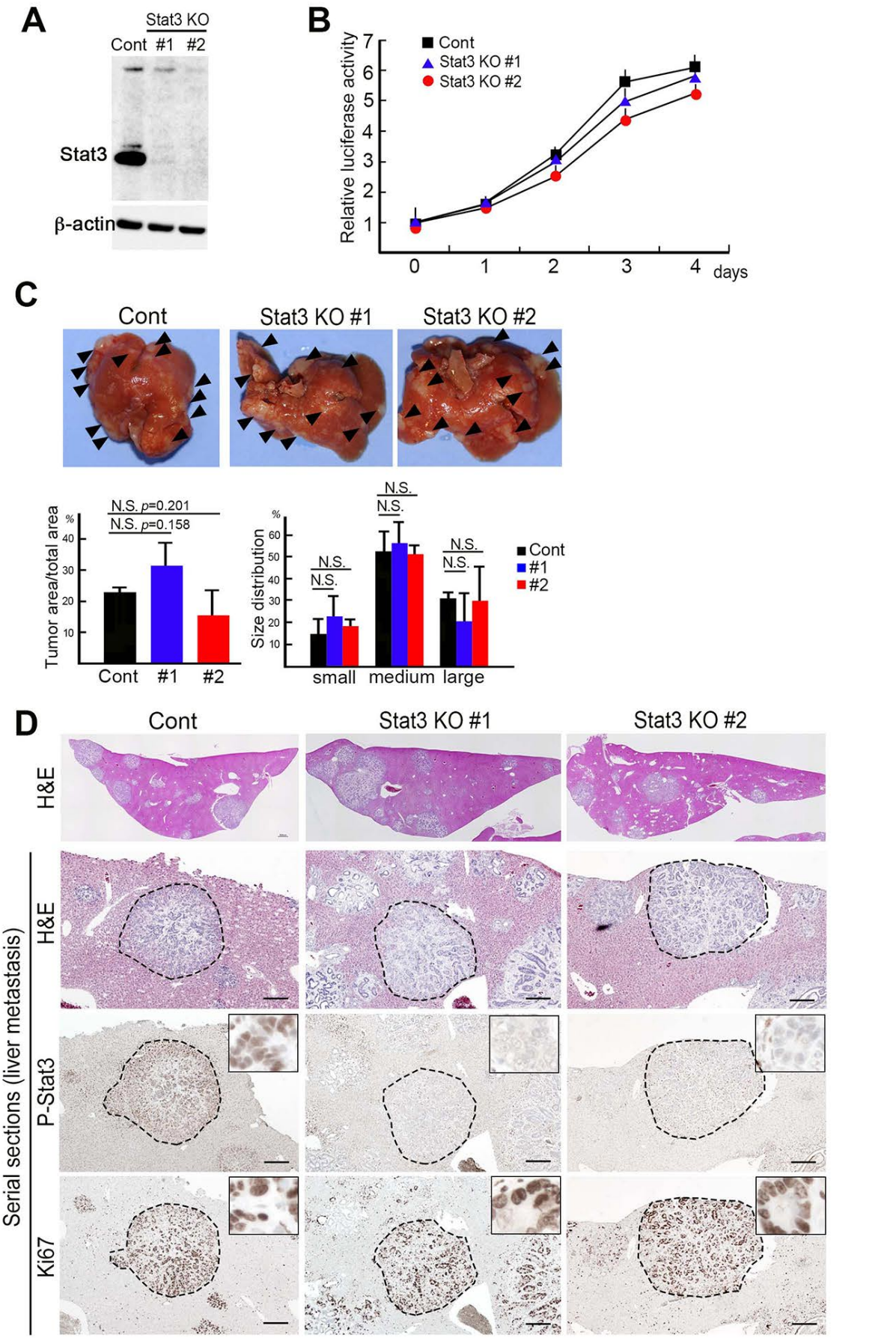
A
Stat3 KO
Cont #1 #2
Stat3
β-actin
B
Relative luciferase activity
Cont
Stat3 KO #1
Stat3 KO #2
days
C
Cont
Stat3 KO #1
Stat3 KO #2
Tumor area/total area
N.S. p=0.201
N.S. p=0.158
Cont #1 #2
Size distribution
N.S.
small medium large
Cont
#1
#2
D
Cont
Stat3 KO #1
Stat3 KO #2
H&E
Serial sections (liver metastasis)
H&E
P-Stat3
Ki67

Figure 6

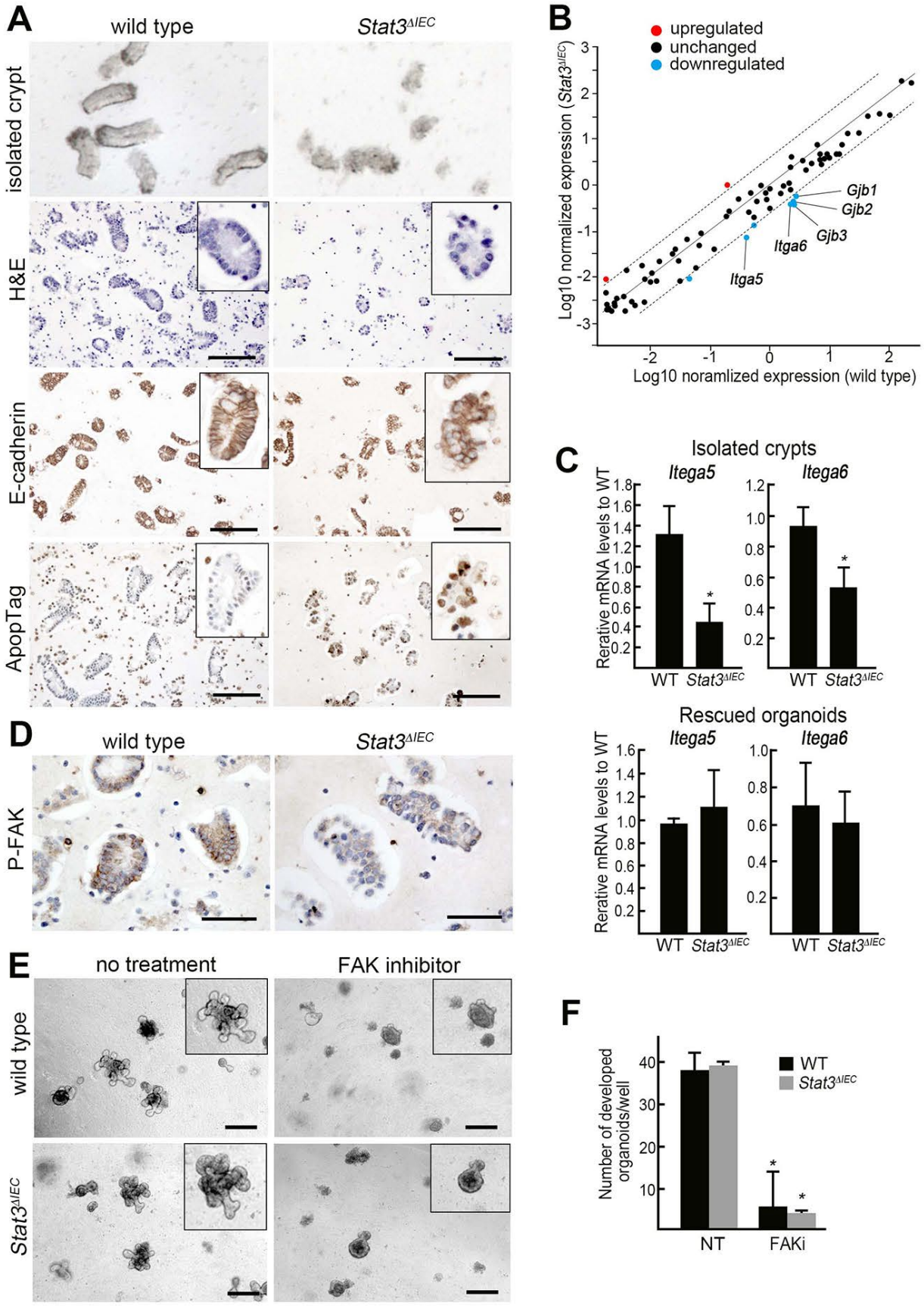
A
wild type
Stat3ΔIEC
isolated crypt
H&E
E-cadherin
ApopTag
B
upregulated
unchanged
downregulated
Log10 normalized expression (Stat3ΔIEC)
Log10 noramlized expression (wild type)
Gjb1
Gjb2
Gjb3
Itga6
Itga5
C
Isolated crypts
Itega5
Itega6
Rerative mRNA levels to WT
WT
Stat3ΔIEC
Rescued organoids
D
wild type
Stat3ΔIEC
P-FAK
E
no treatment
FAK inhibitor
wild type
Stat3ΔIEC
F
Number of developed organoids/well
WT
Stat3ΔIEC
NT
FAKi

Figure 7

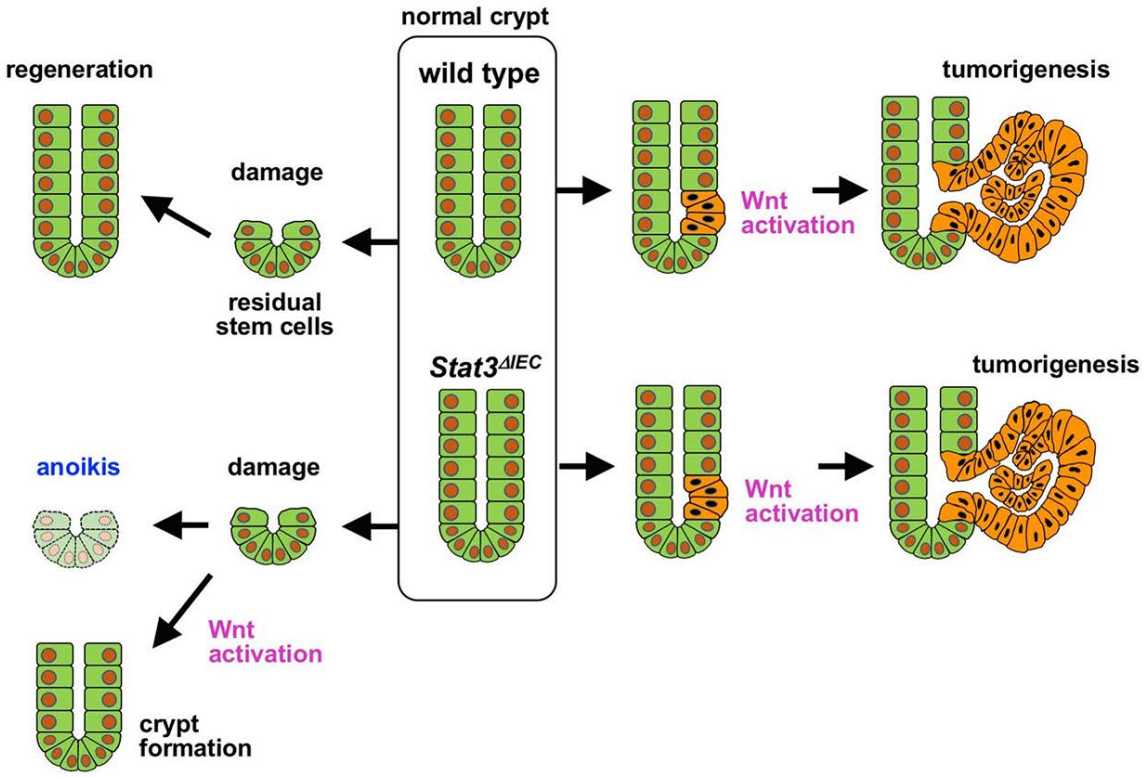
normal crypt
wild type
regeneration
damage
residual
stem cells
Wnt
activation
tumorigenesis
Stat3ΔIEC
anoikis
damage
Wnt
activation
tumorigenesis
Wnt
activation
crypt
formation